

ITERATIVE FINITE ELEMENT DEFORMABLE MODEL FOR NONRIGID COREGISTRATION OF MULTIMODAL BREAST IMAGES

Andrzej Krol^{1,2,3}, Mehmet Z. Unlu², Alphonso Magri³, Edward Lipson^{3,1,2}, Ioana L. Coman^{4,2,1}, James A. Mandel⁵, Karl G. Baum⁶, David H. Feiglin¹

¹Department of Radiology, SUNY Upstate Medical University, Syracuse NY 13210

²Department of Electrical Engineering and Computer Science, Syracuse University, Syracuse NY 13244

³Department of Physics, Syracuse University, Syracuse NY 13244

⁴Department of Mathematics and Computer Science, Ithaca College, Ithaca NY 14850

⁵Department of Civil and Environmental Engineering, Syracuse University, Syracuse NY 13244

⁶Center for Imaging Science, Rochester Institute of Technology, Rochester NY 14623

ABSTRACT

We have developed a nonrigid registration technique applicable to breast tissue imaging. It relies on a finite element method (FEM) model and a set of fiducial skin markers (FSMs) placed on the breast surface. It can be applied for both intra- and intermodal breast image registration. The registration consists of two steps. First, location and displacements of corresponding FSM observed in both moving and target volumes are determined, and then FEM is used to distribute the FSM displacements linearly over the entire breast volume. After determining the displacements at all the mesh nodes, the moving breast volume is registered to the target breast volume using an image-warping algorithm. In the second step, to correct for any residual misregistration, displacements are estimated for a large number of corresponding surface points on the moving and the target breast images, already aligned in 3D, and our FEM model and the warping algorithm are applied again. Our non-rigid multimodality and intramodality breast image registration method yielded good quality images with target registration error comparable with pertinent imaging system spatial resolution.

1. INTRODUCTION

Breast cancer is one of the most common cancers among women in the U.S. [1, 2]. Early detection and treatment are very important for successful breast-cancer treatment and outcome. Previous studies showed that multimodality registration approaches is advantageous in detection and diagnosis of malignant lesions in early stages [3-6]. However, most of these studies were mainly applied to brain or bone images where common rigid surfaces could be easily estimated [7, 8].

In the context of FEM based deformable breast image registration, a number of studies have been recently published. In these studies, mainly large deformations were considered. Samani et al. presented a finite element model based on biomechanical principles to predict breast tissue deformations [9, 10]. Azar et al. [11] has simulated a deformation of the breast to be applied in MRI-guided biopsy. Ruitter et al. [12] registered 3D MR breast volumes and 2D projections of X-ray mammograms using a 3D simulation of the breast deformation based on a biomechanical

model of the mammographic compression. Because physically-based deformable breast models are very difficult to implement [9], we developed a method that does not require information on patient-specific breast morphology and elastic tissue properties. However, it can be applied only if the stress conditions in the imaged breast are virtually the same between moving and target images. This is accomplished by use of identical patient support and positioning systems in both modalities.

2. METHOD

A general block diagram of our method is shown in Fig. 1.

2.1. Fiducial skin markers and their localization

Fiducial skin markers (FSMs) placed on the breast surface are used to sample the displacement between moving and target images (Fig. 2). The locations of the FSMs are marked in ink on the patient's skin to ensure that both types of markers are placed in the same location. The corresponding pairs of markers are manually defined in the target (PET) and in the moving (MRI) images. The localization of markers has been performed by calculating intensity-based centroids, using the method described by Wang et al. [13]. In this iterative knowledge-based method, a user first identifies a voxel belonging to a marker, and then the algorithm finds the lowest threshold, which defines a set of voxels connected in 3D to a selected voxel, thus forming an object with proper geometrical extent in 3D to be a marker. The effective size of the marker is defined by the spatial resolution of the system.

2.2. Construction of patient specific geometry of breast

After performing localization of FSMs and obtaining their displacement vectors, the patient-specific surface geometry of the breast is obtained from MRI images (Fig. 3). First, a simple thresholding is applied to extract the breast volume followed by appropriate closing and opening operations. Finally, the breast surface contours in coronal sections are outlined.

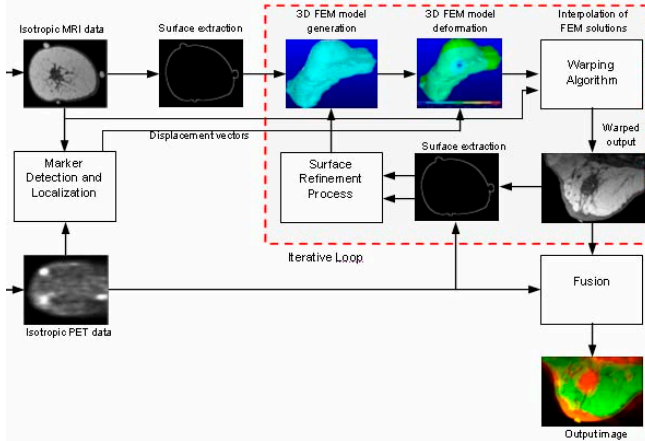


Fig. 1. General block diagram of the method

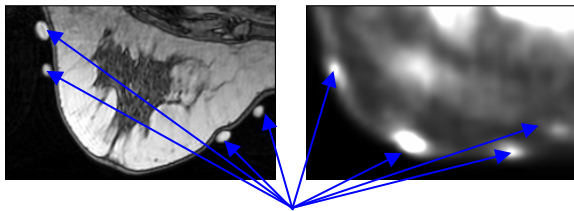


Fig. 2. Fiducial skin markers indicated by arrows visible on MRI and PET breast surfaces in axial view.

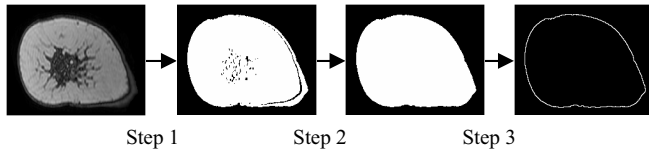


Fig. 3. Construction of patient-specific geometry of breast, using coronal sections of MR breast image.

2.3. FEM model generation in 3D

Our custom written plug-in in ImageJ¹ takes the set of coronal breast contours as input, and generates, in seconds, the 3D finite element method (FEM) file of the breast to be used as an input by FEM software (ANSYS ver. 5.7.1²). The file contains the geometry of the breast built by key points, splines, and volumes as well as the definition of the surface and volume elements, and the displacement vectors. In this study, triangular surface elements and tetrahedral volume elements are used (Fig. 4).

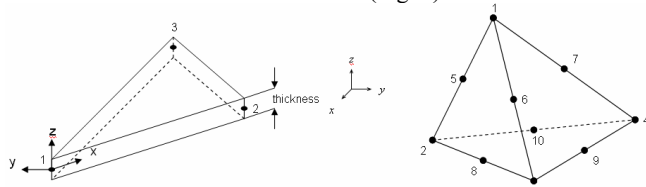


Fig. 4. Triangular thermal shell (left panel) and tetrahedral thermal solid (right panel) mesh elements used in our FEM for the mesh surface and bulk, respectively. The arbitrary thermal conductivity of the shell element is chosen to be 1000 times larger than the tetrahedral element conductivity.

¹ <http://rsb.info.nih.gov/ij/>

² ANSYS, Inc. Canonsburg, Pennsylvania

2.4. FEM model deformation

The breast surface and volume are meshed by a set of finite elements connected through nodes located on element boundaries. A dense displacement field is then obtained using an analogy between displacement vector components and temperature field distribution in steady-state heat transfer (SSHT) in solids, with displacement vectors of FSMs considered analogous to the temperature loads at FSMs. Using the commercial FEM package, the dense displacement field is then estimated, by linearly distributing the Cartesian components of the fiducial displacement vectors first over the breast surface, and then throughout its volume.

2.4. A warping algorithm: Interpolation of FEM solutions

The SSHT FEM computation produces a displacement vector at each node of finite elements. Displacement vectors for each location (voxel or subvoxel) within a finite element can be interpolated using a weighted sum of the element's nodal displacements with the weights equal to the element's node shape function [14],

$$\vec{u} = \sum_{i=1}^{N_{nodes}} N_i^{el} \vec{u}_i^{el} \quad (1)$$

where N_{nodes} is the number of nodes in the element, N_i^{el} is the element's node shape function, and u_i^{el} is the nodal displacement vector. In our study, the exact FEM interpolation given by Eq. 1 is used to obtain the dense displacement field within each FEM element, which in turn is used to interpolate the image gray values via a truncated sinc interpolation kernel. This process is called warping of the moving (floating) image to the target (fixed) image. We emphasize that only the voxels inside the FEM mesh are affected by this kind of processing.

2.5. Refinement via surface-matching algorithm

After obtaining the warped image, a surface-matching algorithm is applied to correct small surface discrepancies for refinement. In this step, instead of using marker displacements, which have already been aligned, we used the displacements at selected corresponding surface points, where there is a registration problem, to determine the transformation between the two images. For this purpose, surface regions, which need to be refined, are first determined and represented by the curves in 2D, using cubic-spline representations on moving and target images. Then, using the closest distance criterion, the corresponding points on the target image surface are determined for each of the selected points on the moving image. Using the distances between the corresponding points on moving and target images, and with the application of our FEM model, the moving image is deformed a second time. Finally, using the same analogy and the method described above, the displacements are distributed over the entire volume and then the two images are registered using the warping algorithm again.

3. EXPERIMENTAL STUDY

Data from 12 subjects were acquired using a dedicated PET/CT scanner (GE Discovery ST with BGO detector and 4-slice CT) and

a 1.5 T MRI system (Philips Intera). PET images were obtained with patient prone and breasts freely suspended, immediately after intravenous administration of 10 mCi of F-18-FDG with nine FSMs taped on each breast. They were reconstructed in a $128 \times 128 \times 47$ matrix, with 4.25 mm voxel size. Each FSM contained 0.5 μ Ci of Ge-68. To assure that the stress conditions in the imaged breast are virtually the same in different modalities, a replica of the MRI breast antenna made of plastic with very low absorption for 511 keV photons in PET scans was used. In MRI scans, the patient was prone with both breasts suspended into a single well housing a standard Philips clinical breast RF receiver coil. A high-resolution 3D Fast Field Echo (FFE) technique with TR/TE = 14/3 was applied to obtain MRI breast images. An image matrix of $512 \times 512 \times 120$ was used in reconstruction with $0.7 \times 0.7 \times 1.4$ mm³ voxel size. The field of view (360 mm \times 360 mm) was centered over the breasts.

In the following examples, coregistered images are fused using a frame-by-frame approach; a “fire” pseudo color scheme was used to display low resolution functional F-18-FDG PET data, and gray scale was used to display high resolution anatomical MRI data. After applying these color schemes, the resulting images are averaged with equal weight.

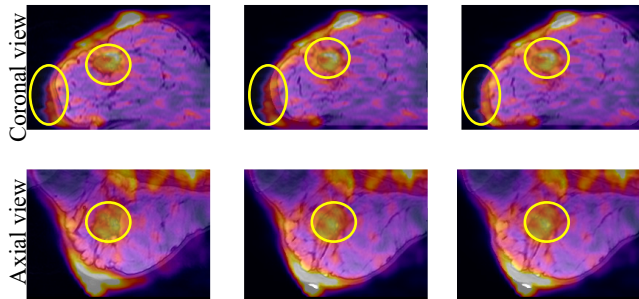


Fig. 5. Comparison of fused images of Subject 1. Left: After rigid registration. Middle: After first iteration. Right: After second iteration. The region of interest is circled with yellow line.

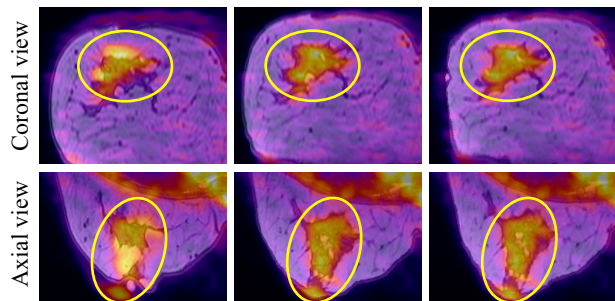


Fig. 6. Comparison of fused images of Subject 2. Left: After rigid registration. Middle: After first iteration. Right: After second iteration. The region of interest is circled with yellow line.

4. EVALUATION OF THE RESULTS

We tested our results using both qualitative and quantitative methods. To test and compare our results qualitatively, we implemented three different similarity measurement plots named isoprojected surface similarity (ISS), normalized polar surface similarity (NPSS) and z-axis surface similarity (ZSS). The ISS plot is a surface projection image, which represents normalized distances between the corresponding points on the surfaces with

the same z-axis coordinate as an intensity value. ISS gives the opportunity to determine where the two images are aligned well or not (Fig. 7). An NPSS plot is similar to an ISS plot, except that it is a polar isoprojection of the normalized distances between the corresponding points on the surfaces, and the center of it corresponds to the apical section of the imaged breast. NPSS has the advantage of allowing comparison of different patients (Fig. 8). ZSS is a two dimensional graph which represents the average and maximum surface differences for each slice between the target and moving images, before and after application of our nonrigid registration method, as well as after rigid registration (Fig. 9). To test our results quantitatively, mutual information and normalized mutual information (NMI) were calculated before and after application of our non-rigid registration method (Table 1). We also performed error analysis to investigate how our method behaves when the number of FSMs was changed (Table 2), and how much error is introduced when the fiducial markers are localized with different amounts of errors (Table 3).

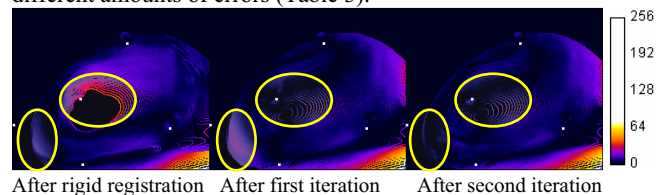


Fig. 7. ISS – Isoprojected surface similarity plot for Subject 1 to compare surface differences for each point at the corresponding slice. The region of interest is circled with yellow line.

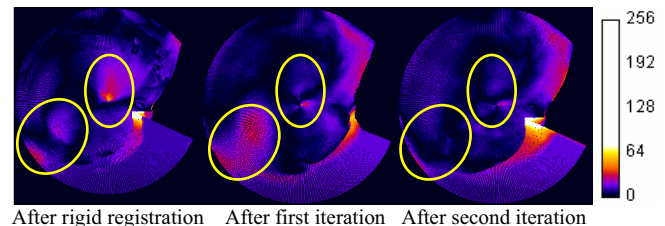


Fig. 8. NPSS – Normalized polar surface similarity plot for Subject 1 to compare surface differences for each point in the same angle with respect to apex center at the corresponding slice. The region of interest is circled with a yellow line.

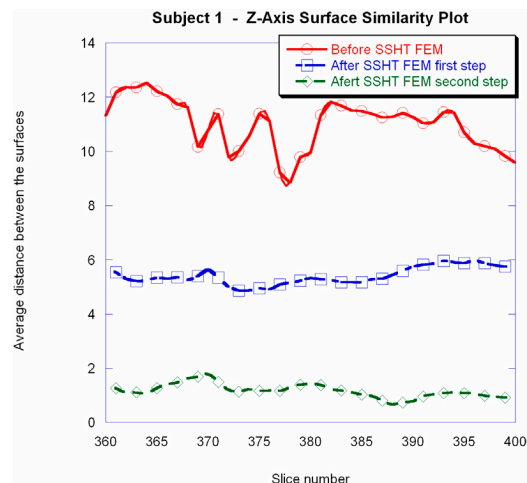


Fig. 9. Z-axis surface similarity plot to compare average and/or maximum surface differences for each corresponding slice.

Table 1. Calculated image similarity measures for multimodal registration.

Subject	After rigid reg.		After 1 st step		After 2 nd step	
	MI	NMI	MI	NMI	MI	NMI
1	1.22	1.10	2.63	1.22	2.85	1.24
2	1.48	1.12	2.09	1.17	2.26	1.19
3	1.40	1.12	1.56	1.13	1.39	1.11
BEST	Max.	2	Max.	2	Max.	2

Table 2. Average target registration error (TRE) vs. number of fiducial skin markers.

Subject		Average target registration errors [mm]					
		Number of markers used:					
		ROIs inside or outside the polyhedron	9	7	5	4	3
1	After 1 st iteration	Outside	2.02	2.56	2.57	2.63	2.80
		Inside	0.84	1.27	1.28	1.53	1.97
	After 2 nd iteration	Outside	1.38	1.65	1.30	1.33	1.68
		Inside	0.48	0.70	0.69	1.07	1.27

Table 3. Average target registration error (TRE) vs. fiducial localization error (FLE).

Subject		Average target registration errors [mm]				
		Errors introduced ($\epsilon = 1.7$ mm)				
		ROIs inside or outside the polyhedron	$0 \times \epsilon$	$1 \times \epsilon$	$2 \times \epsilon$	$3 \times \epsilon$
1	After 1 st iteration	Outside	2.02	2.33	2.73	3.20
		Inside	0.84	1.15	1.67	2.27
	After 2 nd iteration	Outside	1.38	1.20	1.39	2.03
		Inside	0.48	0.54	0.72	0.99

5. CONCLUSION

Our coregistration method requires external FSMs and a system for careful breast positioning to prevent changes in internal stress conditions between modalities. We tested our model on 12 subjects with FSMs, imaged using PET and MRI. Using the selected region of interests (ROI), we estimated the target registration error to be less than two PET voxels (1–6 mm depending on location in the breast). The results showed that our nonrigid multimodality and intramodality breast-image registration method yielded good quality images with target registration error comparable with the spatial resolution of the pertinent imaging system.

ACKNOWLEDGMENTS

This research was sponsored in part by a Carol M. Baldwin Breast Cancer Research Award.

REFERENCES

[1] Boring, C.C., et al., *Cancer Statistics*. Ca: a Cancer Journal for Clinicians, 1994. **44**(1): p. 7-26.
 [2] Society, A.C. *What Are the Key Statistics for Breast Cancer?* <http://www.cancer.org>. [Web Page] 2004 [cited 2004].

[3] Somer, E.J., et al., *PET-MR image fusion in soft tissue sarcoma: accuracy, reliability and practicality of interactive point-based and automated mutual information techniques*. European journal of nuclear medicine and molecular imaging, 2003. **30**(1): p. 54-62.
 [4] Makela, T., P. Clarysse, and O. Sipila, *A Review of Cardiac Image Registration Methods*. IEEE Transactions on medical imaging, 2002. **21**: p. 1011-1021.
 [5] Buscombe, J.R. and I. Khalkhali, *Scintimammography with Single-Photon Tracers.*, in *Nuclear Oncology: Diagnostic and Therapy*, I. Khalkhali, J. Maublant, and S.J. Goldsmith, Editors. 2001, Williams & Wilkins: Philadelphia. p. 273-287.
 [6] Sailer, S.L., et al., *Improving treatment planning accuracy through multimodality imaging*. International journal radiation oncology, 1996. **35**: p. 117-124.
 [7] Barra, V. and J.Y. Boire, *A General Framework for the Fusion of Anatomical and Functional Medical Images*. NeuroImage, 2001. **13**: p. 410-424.
 [8] Maintz, J.B.A. and M.A. Viergever, *A Survey of Medical Image Registration*. Medical Image Analysis, 1998. **2**(1): p. 1-36.
 [9] Samani, A., et al., *Biomechanical 3-D finite element modeling of the human breast using MRI data*. IEEE Trans Med Imaging, 2001. **20**(4): p. 271-9.
 [10] Wellman, P.S., *Tactile imaging*. 1999, Harvard University: Cambridge MA.
 [11] Azar, F.S., *A Deformable Finite Element Model of the Breast for Predicting Mechanical Deformations under External Perturbations*, in *BioEngineering*. 2001, Univeristy of Pennsylvania: Philadelphia, PA. p. 208.
 [12] Ruiter, N.V., *Registration of X-ray Mammograms and MR-Volumes of the Female Breast based on Simulated Mammographic Deformation*. 2003, Universitat Mannheim: Mannheim. p. 153.
 [13] Wang, M.Y., et al., *An automatic technique for finding and localizing externally attached markers in CT and MR volume images of the head*. Biomedical Engineering, IEEE Transactions on, 1996. **43**(6): p. 627 -637.
 [14] Zienkiewicz, O.C. and R.L. Taylor, *The Finite Element Method*. 1987, New York: McGraw Hill Book Co.